EXPERIMENTAL STUDY ON EVAPORATION OF DEFROSTING RESIDUAL DROPLET ON FIN SURFACE AND ENHANCEMENT BY ELECTRIC FIELD

by

Mengting XIANG, Feng WANG*, and Fei DAI

College of Electrical, Energy and Power Engineering, Yangzhou University, Yangzhou, China

Original scientific paper
https://doi.org/10.2298/TSCI250915219X

In order to improve defrosting efficiency of air source heat pump, it is crucial to reveal the evaporation characteristics of defrosting residual droplet on fin surface and find ways to enhance the evaporation performance. In this work, the evaporation of defrosting residual droplet is investigated experimentally under different influence factors according to the defrosting condition of air source heat pump. Meanwhile, the availability of the evaporation performance enhanced by electric field is evaluated. Experimental results show that the droplet evaporates on superhydrophobic fin surface at constant contact angle and mixed modes, without the pinning stage; while it is constant contact diameter and mixed modes on bare fin surface. As the fin surface temperature increases or the droplet size decreases, the evaporation time of the droplet becomes shorter. The droplet evaporation time is 25.4% of that without electric field on bare fin surface, when the droplet volume is 1 μL and the electric intensity is 15 kV/cm. Interestingly, the electric field forces the droplet on superhydrophobic fin surface to jump, and it is no longer necessary to remove the droplet by evaporation. In a word, applied electric field can enhance the droplet evaporation, which will save defrosting energy consumption and improve defrosting efficiency of air source heat pump.

Keywords: *air source heat pump, defrosting residual droplet, evaporation, superhydrophobic surface, electric field*

Introduction

Air source heat pump (ASHP) has the advantages of cooling and heating, energy saving, environmental protection, flexible installation and so on [1]. It is widely used as cooling and heating sources for building air conditioning. However, there is frosting phenomenon on the surface of the outdoor finned tube heat exchanger when ASHP is used for heating in winter. The frost layer can decrease the heating capacity of ASHP by 15%-25% and reduce its heating efficiency by 10.7%-20.9%, seriously affecting its heating performance and stable operation [2]. Although researchers have put forward various anti-frosting methods [3, 4], such as air dehumidification by desiccant, ultrasonic vibration, and surface treatment, frosting cannot be avoided and defrosting needs to be carried out for ASHP in time. In the defrosting process, the refrigerant condenses in the outdoor heat exchanger to release heat and melt the frost layer. Due

*Corresponding author, e-mail: wfeng@yzu.edu.cn

to the adhesion of the fin surface, the defrosting water cannot be completely drained away. The defrosting water that remains on the fin surface will freeze directly during the next frosting process, and even form *permafrost zone* [5]. To evaporate the residual water, not only additional energy needs to be consumed, but also defrosting time is significantly extended. Therefore, it is very important to reveal the evaporation characteristics and rules of defrosting residual droplet on fin surface, and put forward suitable method to enhance evaporation performance, so as to save defrosting energy consumption and improve defrosting efficiency.

The evaporation of defrosting residual droplet on fin surface is similar to that of sessile droplet on heated surface. Current researches have systematically investigated the droplet evaporation mode on solid surface and the influence factors of droplet evaporation. Droplet evaporation on solid surface typically involves two fundamental modes [6]: the constant contact radius (CCR) mode, characterized by gradually decreasing contact angle with CCR and the constant contact angle (CCA) mode, where the contact angle remains constant while the contact radius continuously decreases. In practice, droplet evaporation often follows a complex pattern, typically initiating in the CCR mode before transitioning to a mixed mode characterized by the simultaneous decrease of both contact angle and contact radius. Stick-slip behavior was observed during droplet evaporation experiments [7]. In this mode, the droplet initially evaporates in the CCR mode until capillary force imbalance occurs. This imbalance triggers stick-slip motion of the three-phase contact line, which subsequently re-establishes equilibrium and initiates a new cycle of this mode. Dietrich *et al*. [8] studied the evaporation of hexanol droplet and found that when the contact angle of a micro-liter-volume droplet was less than 90°, the evaporation process exhibited a stick-jump phenomenon.

There are many factors that affect the droplet evaporation, including environmental parameters, physical and chemical properties of droplet, temperature and wettability of solid surface. Girard *et al*. [9] studied the influence of substrate temperature and ambient humidity on droplet evaporation, and the results showed that the increase of substrate temperature improved the evaporation efficiency, while the relative humidity had a strong effect only when the substrate temperature was below 50 °C. Fukatani *et al*. [10] found that self-generated thermal patterns were enhanced by increasing ambient temperature or decreasing humidity. In addition, the evaporation rate was affected by the convection of ambient air and the droplet life decreased with the increase of air velocity [11, 12]. Sefiane *et al*. [13] found in experiments that significant reduction in atmospheric pressure greatly increased the droplet evaporation rate. There are significant differences in droplet evaporation efficiency and evaporation mode on various wetting surfaces [14]. Dash and Garimella [15] found that the droplet evaporation on hydrophobic surface was dominated by CCA mode. The stronger the hydrophobicity of the solid surface is, the more likely the droplet evaporation is to appear CCA mode. Therefore, droplet evaporation on superhydrophobic surface mostly follows the CCA mode [16].

Since droplet evaporation on solid surface is a critical process in various industrial applications, there is an increasing effort to enhance droplet evaporation performance. The addition of an electric field is considered as an appropriate method to enhance evaporation performance with low power consumption [17]. Furthermore, the shape, contact angle and wetted area of the droplet all changed under the action of electric field [18]. Scholars found that electric field enhanced droplet evaporation in the following three ways [19]: increasing the evaporation surface area by droplet deformation under the action of electric field, improvement in the heat transfer efficiency between the droplet and the solid surface due to the internal vortex, and enhanced the shear effect on the vapor layer by external vortex.

Current researches have fully expounded droplet evaporation characteristics on solid surface and revealed the availability and mechanism of droplet evaporation enhanced by electric field. However, the research object of this paper is defrosting residual droplet on fin surface when ASHP is used for heating in winter. Factors affecting droplet evaporation characteristics, such as droplet size (0-2 mm), properties of solid surface (Al), heating temperature (< 50 °C) and environmental parameters (< 5 °C), are significantly different from those of current researches. In particular, the environmental conditions of current researches are mainly room temperature or high temperature (> 20 °C), while the evaporation of defrosting residual droplet is in a low temperature environment in winter climate. In addition, studies showed that designing fin structures [20] or improving frosting uniformity [21] can facilitate the drainage of defrosting water and reduce its retention, however, there is no investigation on how to enhance the evaporation performance of defrosting residual droplet. Due to the differences between the environmental conditions of current researches and the defrosting conditions of ASHP, the availability and mechanism of electric field on enhancing the evaporation performance of defrosting residual droplet need to be further evaluated and revealed.

In this paper, the evaporation characteristics of defrosting residual droplet are investigated experimentally under different influence factors according to the defrosting condition of ASHP in winter, and the availability and mechanism of the evaporation performance enhanced by electric field are evaluated and revealed. The experimental results will have guiding significance to save defrosting energy consumption and improve defrosting efficiency of ASHP.

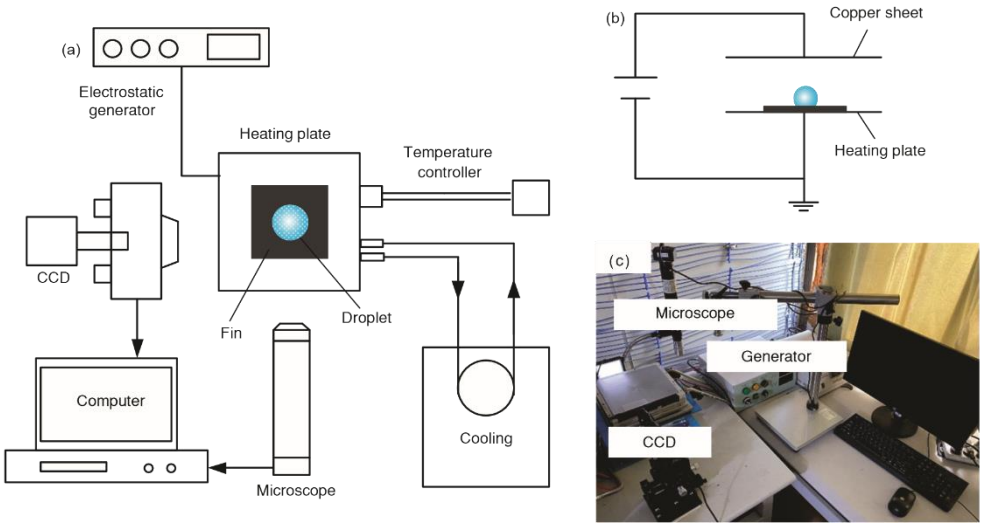

Figure 1. Experimental devices; (a) schematic diagram of experimental platform of droplet evaporation on fin surface with electric field applied, (b) schematic diagram of plate electrode device, and (c) physical drawing of experimental platform

Experimental method

Experimental devices

Figure 1 shows experimental devices. In fig. 1(a), the heating plate (model: SLTD1-600S) with semiconductor refrigeration is used to control the temperature of the fin surface, so

that the droplet on the fin surface evaporates at a constant temperature. The temperature of the heating plate can be controlled from –30-60 °C. The CCD camera (model: ZOOM-600TR) and the microscope (model: YXC-0745CT) are used to observe and record the side and the front images of the droplet respectively, and transmit the images to the computer. Droplets are picked up using an automatic micropipettor (maximum random error 0.8%) with measuring range from 0.5-10 μL. The electrostatic generator is used to provide a stable electric field, and the maximum voltage that the device can provide is 15 kV. Figure 1(b) shows the schematic diagram of the plate electrode device. The lower plate of the electrode is the surface of the heating plate and is grounded. The upper plate is a copper sheet (size: 70 mm × 30 mm × 1 mm) connected to the output end of the electrostatic generator. The spacing of the plates in the experiments is 10 mm.

Preparation and characterization of fin surface

To achieve the effect of wettability of fin surface on evaporation characteristics of droplet, bare and superhydrophobic fin surfaces (SFS) are used for comparative experiments. A pure aluminum sheet with a size of 70 mm × 30 mm × 1 mm (length × width × thickness) is used as the bare fin. The superhydrophobic fin is obtained by surface modification of bare fin. Figure 2(a) shows the schematic diagram of preparation of superhydrophobic fin. The superhydrophobic fin was prepared by coating spraying method previously used: first, the bare aluminum fin is cleaned; then, SiO_2 superhydrophobic coating solution is prepared; finally, a spray gun is used to spray the coating on the fin surface. Under the pressure of 0.6 MPa, the spray gun was carried out *S*-shaped spraying from the top to the bottom of the aluminum surface at a speed of 3 cm/s and a spraying spacing of 10 cm. The surface contact angles of the superhydrophobic fin and the bare fin are measured to be 161° and 75°, respectively. The surface temperatures of bare and superhydrophobic fins were measured using thermocouples when the surface temperature of the heating plate was 40 °C. The results showed that the temperature difference between the two types of fins was 0.6 °C, ensuring the validity of the comparison in the evaporation experiments.

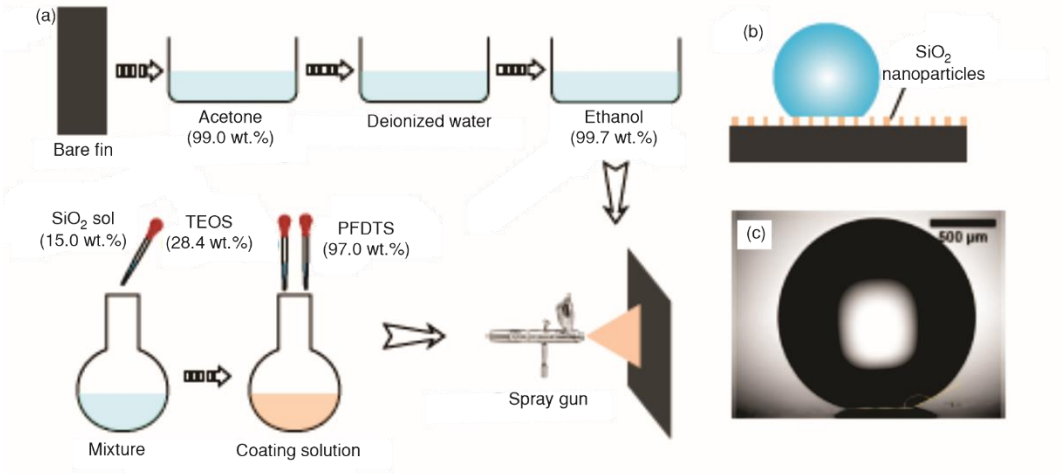

Figure 2. Preparation and characterization of superhydrophobic fin; (a) preparation process, (b) schematic diagram of droplet on SFS, and (c) contact angle

Experimental conditions

There are two experiments in this study, one is the droplet evaporation characteristics under different influence factors, and the other is the enhancement of droplet evaporation by electric field. The details of experimental conditions are illustrated in tab. 1, which are chosen according to the defrosting condition of ASHP. The experimental platform of droplet evaporation is placed in an experimental chamber, and the air temperature and relative humidity in the experimental chamber are controlled by air conditioning and humidifier. It should be explained that due to the limited cooling capacity of the air conditioning, the lowest air temperature can be created is 5 °C. Therefore, the environmental temperature condition is set at 5 °C. The droplet morphological parameters (contact angle, contact diameter, height, *etc*.) averaged over three repeated experiments. The measurement errors of all the measurement parameters in the experiments are shown in tab. 2..

Table 1. Parameters of experimental conditions

	Parameter	Value
Constant	Environmental temperature [°C]	5
	Environmental relative humidity [%]	60
Variable	Droplet volume [μL]	1, 1.1, 1.4, 1.7, 2, 3
	Fin surface [bar]	Superhydrophobic
	Heating temperature [°C]	30, 35, 40
	Electric intensity [kVcm^{-1}]	0, 5, 10, 15

Table 2. Measurement errors of measurement parameters

Parameter	Instrument	Uncertainty
Environmental temperature	Digital temperature-humidity sensor	±0.3 °C
Relative humidity		±2%
Surface temperature	*T*-type thermocouple	±0.2 °C
Droplet volume	Micropipettor	±0.8%
Contact angle	ImageView software	±1%
Contact diameter		±0.01 mm
Droplet height		±0.01 mm

Experimental results and discussion

Droplet evaporation characteristics under defrosting condition of ASHP

The droplet evaporation characteristics on the bare fin surface (BFS) and SFS are compared. The droplet volume is 1.7 μL and the heating temperature of the fin surface is 40 °C. Figure 3 shows the comparison of droplet evaporation on BFS and SFS. Figure 3(a) shows the visualization of droplet evaporation under normalized time scale. The normalized time is defined as the ratio of a moment, t, during the droplet evaporation process to the total droplet lifetime, t_m). In fig. 3(a), the droplet appears roughly hemispherical on BFS and almost spherical on SFS at the initial stage of evaporation. As evaporation proceeds, the droplet shape on BFS changes to flat shape, while the droplet on SFS remains in a superhydrophobic state in 90% evaporation time. In the last stage, the droplet on SFS is fan-shaped until the droplet evaporates completely. Figure 3(b) shows the changes of contact angle (left), contact diameter (middle), and droplet height (right) of droplet with time on BFS and SFS. It is seen that the change rules

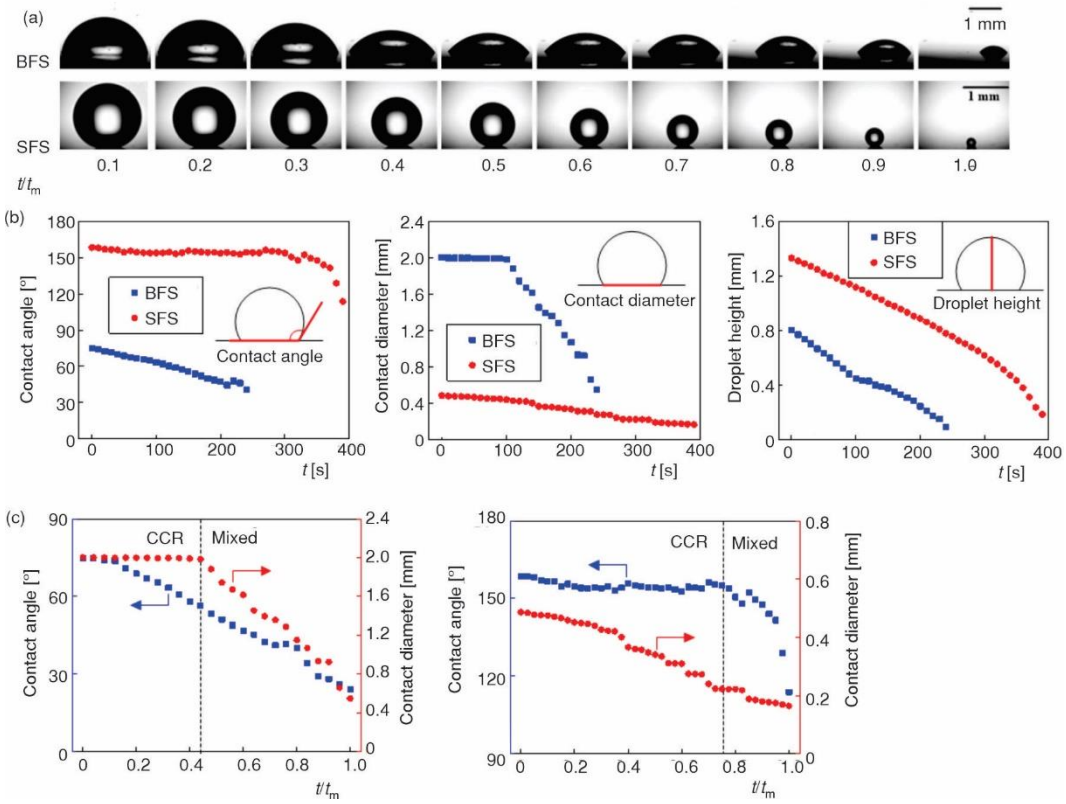

Figure 3. Comparison of droplet evaporation on BFS and SFS;
(a) visualization of droplet evaporation,
(b) changes of contact angle (left), contact diameter (middle), and droplet height (right) with time, and
(c) changes of contact angle and contact diameter on BFS (left) and
SFS (right) under normalized time scale

of contact angle and contact diameter are quite different on BFS and SFS, while the variation trend of droplet height is similar. The contact angle of droplet on BFS decreases gradually during the evaporation process. However, the contact angle of droplet on SFS changes very little in the first 80% evaporation time and keeps above 150°, and then decreases in the last 20% evaporation time. As for contact diameter, it decreases gradually during the evaporation process on SFS, while it remains almost constant on BFS in the first 40% evaporation time, and suddenly decreases in the last 60% evaporation time. In addition, droplet on SFS takes longer to evaporate than on BFS. The value of tm on BFS and SFS is about 250 seconds and 400 seconds, respectively. The changes of contact angle and contact diameter of droplet on BFS and SFS under normalized time scale are shown in fig. 3(c). The droplet on BFS evaporates in CCR mode in the first 40% evaporation time, and then switches to mixed mode. However, the droplet on SFS evaporates in CCA mode in the first 80% evaporation time, and then switches to mixed mode. Since the evaporation mode of droplet on BFS is CCR mode at the initial stage, the contact angle decreases linearly, and the droplet is in a pinned state. The hysteresis of the three-phase contact line and surface excess free energy of the droplet on BFS are small, so that the droplet can quickly transfer to depinning state and completely evaporate in a short time. However, no pinning phenomenon is observed on SFS.

The heating temperature of the fin surface is 30 °C, 35 °C, and 40 °C. The droplet volume is 1.7 μL. Figure 4 shows the droplet evaporation on SFS under different heating temperature. Figure 4(a) shows the visualization of droplet evaporation under normalized time scale. With the increase of heating temperature, the evaporation rate of the droplet increases. Under different heating temperatures, the droplet shape changes in the same way, and the droplet changes from spherical to fan-shaped. However, the increase of heating temperature will accelerate the evaporation process, leading to an earlier change in droplet shape. Figure 4(b) shows the changes of contact angle (left), contact diameter (middle), and droplet height (right) of droplet with time. It is seen that the variation trends of the parameters under different heating tem-

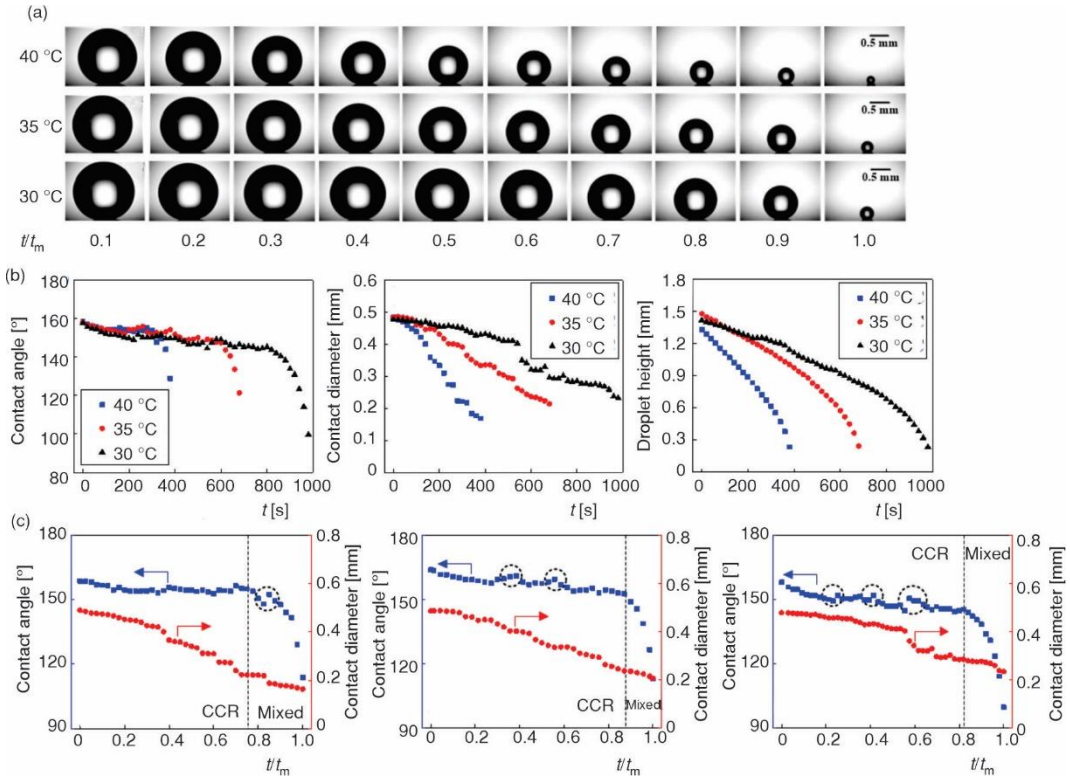

Figure 4. Droplet evaporation on SFS under different heating temperature;
(a) visualization of droplet evaporation,
(b) changes of contact angle (left), contact diameter (middle), and droplet height (right) with time, and
(c) changes of contact angle and contact diameter with 40 (left), 35 (middle), and 30 °C (right) heating temperature under normalized time scale

peratures are consistent, but the changing rate is different due to the difference of droplet evaporation rate. Taking the droplet height as an example, the droplet height decreases with time under different heating temperatures. When the heating temperature is 35 °C, the droplet height is decreased by 60.8% from 1.48-0.58 mm in the first 600 seconds of the evaporation process. When the heating temperature is 30 °C, the droplet height is decreased only by 35.2% from 1.42-0.92 mm. The changes of contact angle and contact diameter of droplet under normalized time scale are shown in fig. 4(c). It is seen that when the heating temperature is 40 °C, the droplet first evaporates in CCA mode, and then switches to mixed mode. At 35 °C and 30 °C,

the change of evaporation mode is basically the same as that at 40 °C. However, when the heating temperature is 40 °C, the droplet contact diameter shrinks faster, the proportion of CCA mode in evaporation process decreases, and the proportion of mixed mode becomes longer. When the temperature is 35 °C and 30 °C, the droplet evaporation switches to mixed mode at about 630 seconds and 820 seconds, respectively. Compared with 40 °C, the switched time is shortened by 280 seconds and 470 seconds, respectively. When the heating temperature decreases, the sudden increase of droplet height is observed when the droplet shrinks, so that the contact angle increases suddenly. As seen by the black dashed boxes in fig. 4(c), the periodic *stick-jump* phenomenon occurs: the contact diameter shrinking, the contact angle and the droplet height increasing abruptly. The lower the heating temperature, the more obvious this phenomenon becomes. As the heating temperature decreases, the droplet evaporation rate slows down, intensifying the competition between pinning at the three-phase contact line and the surface tension-driven shrinkage. Under lower temperature, reduced evaporation prolongs contact line pinning, allowing the droplet to accumulate surface energy through continuous contact angle reduction. When the energy exceeds the critical pinning force threshold, the contact line abruptly retracts, causing sudden jumps in contact angle. The slower evaporation allows more sufficient energy accumulation, resulting in more pronounced periodic *stick-jump* phenomenon. By comparison the evaporation time of droplet on SFS under different heating temperature, it is seen that with the increase of heating temperature, the evaporation time of droplet becomes shorter. When the heating temperature is 30 °C, the t_m is 990 seconds. As the temperature rises to 40 °C, the t_m decreases to 400 seconds, which reduces the survival time of droplet on fin surface by 59.5%.

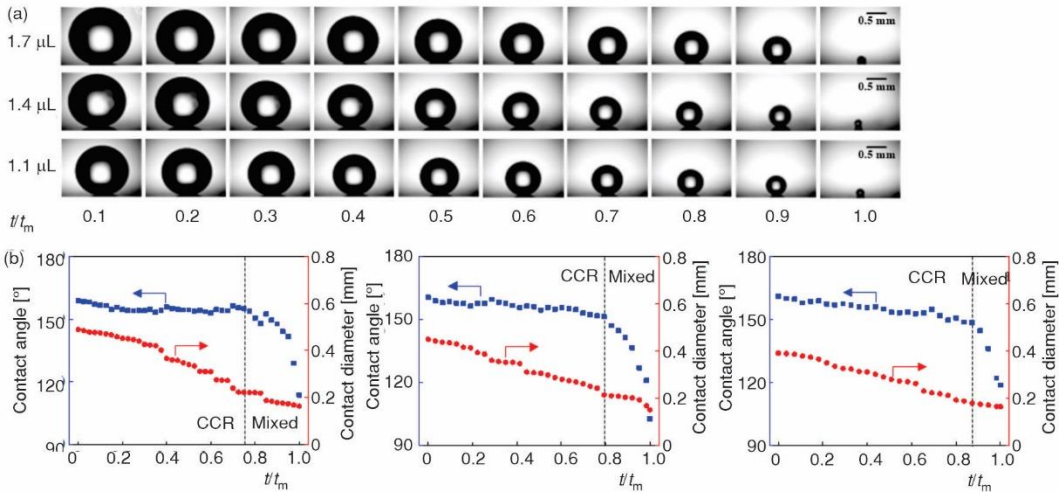

Figure 5. Evaporation of droplet with different volume on SFS;
(a) visualization of droplet evaporation and (b) changes of contact angle and contact diameter with 1.7 (left), 1.4 (middle), and 1.1 μL (right) droplet volume under normalized time scale

The droplet volume is 1.1 μL, 1.4 μL, 1.7 μL. The heating temperature of the fin surface is 40 °C. Figure 5 shows the evaporation of droplet with different volume on SFS. As seen from fig. 5(a), during most of the evaporation process, the droplet on SFS is spherical crown. With the decrease of droplet volume, the evaporation rate of the droplet increases, but its shape changes consistently. The changes of contact angle and contact diameter of droplet under normalized time scale are shown in fig. 5(b). By comparison the droplet evaporation time

with different volume on SFS, it is seen that with the increase of droplet volume, the evaporation time of droplet decreases. When the droplet volume is 1.7 μL, the tm is 400 seconds. As the droplet volume is 1.1 μL, the tm decreases to 319 seconds, which reduces the droplet lifetime by 20.3%. As the volume of the droplet decreases, the proportion of the mixing stage in the entire evaporation process decreases. However, the droplet with smaller volume enters the mixing stage earlier. When the droplet volume is 1.1 μL, the time required to enter the mixing stage is 280 seconds, whereas for a droplet volume of 1.7 μL, this time increases to 302 seconds.

Enhancement of droplet evaporation by electric field

We found that the droplets showed completely different behaviors on BFS and SFS. On BFS, the electric field enhances the evaporative performance, while the droplet bounces off the SFS, thus omitting the subsequent evaporation process. Figure 6 shows the enhance effect and mechanism of droplet evaporation on BFS by electric field. The evaporation time of droplet with different volume under different electric intensity is presented in fig. 6(a). On the one hand, with the increase of electric intensity, the evaporation time of the droplet is shortened. This shows that the applied electric field can improve the efficiency of droplet evaporation. However, the improvement degree of evaporation efficiency is different with different electric intensity. When the droplet volume is 1 μL and the electric intensity is 5 kV/cm, the average evaporation time is 280 seconds, which is about 94.9% of the natural evaporation time. When the electric intensity is 15 kV/cm, the average evaporation time is only 75 seconds, which is about 25.4%

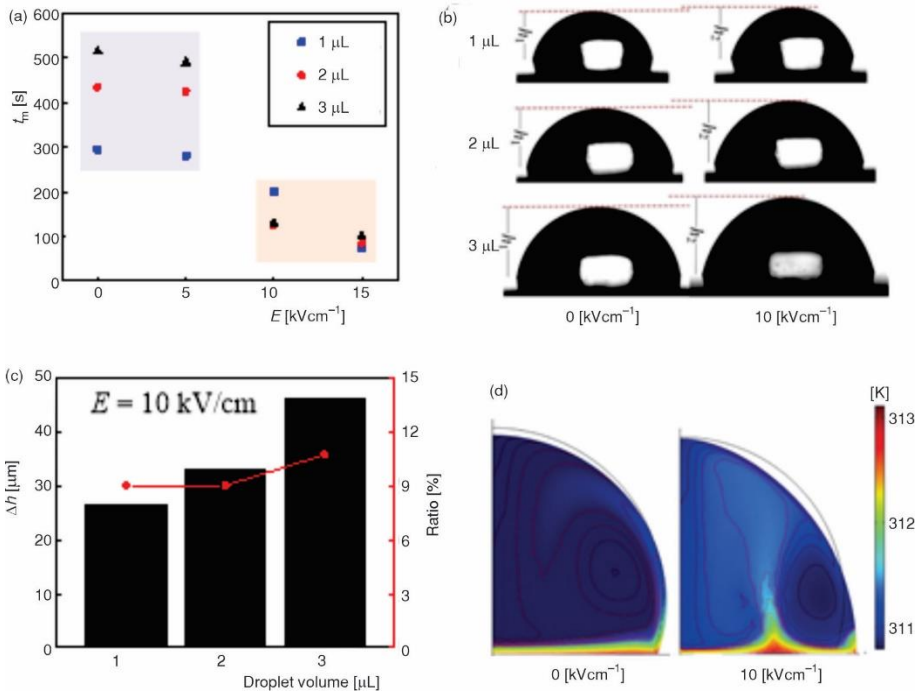

Figure 6. Enhancement of droplet evaporation on BFS by electric field;
(a) evaporation time of droplet with different volume under different electric intensity,
(b) visualization of droplet deformation under electric intensity of 10 kV/cm,
(c) absolute value and ratio of change in droplet height, and
(d) temperature field distribution inside droplet

of the natural evaporation time. On the other hand, the larger the droplet volume, the more obvious the electric field is in enhancing droplet evaporation. When the droplet volume is 3 μL and the electric intensity is 15 kV/cm, the average evaporation time is 100 seconds, which is about 19.4% of the natural evaporation time. Compared with the droplet volume of 1 μL, the shortening of evaporation time is more significantly.

Under the action of electric field, the charge distribution on the droplet surface is uneven, and the charges will repel each other, causing coulomb repulsion and reducing the surface tension of the droplet. The decrease in surface tension means that the adhesion of the droplet on the fin surface weakens, making the droplet more prone to deformation, as shown in fig. 6(b), thereby increasing the contact area between the droplet and the atmosphere, enhancing the convective heat transfer, and then improving the evaporation rate of droplet. Figure 6(c) shows the absolute value and ratio of change in droplet height when the electric intensity is 10 kV/cm. When the droplet volume is 3 μL, the droplet height increases by 10.8% from 429.5-475.7 μm. When the droplet volume is 1 μL, the droplet height increases by 9.1%. It is seen that the larger the droplet volume, the more significant the droplet deformation. In addition, the electric field promotes the flow inside the droplet, which also affects the heat transfer inside the droplet. In fig. 6(d), when the heating temperature is 40 °C, the moment of the first second of droplet evaporation process is selected, and the temperature field distribution inside the droplet is compared when there is no electric field and the electric intensity is 10 kV/cm. When there is an electric field, the flow rate inside the droplet increases significantly, and the fluid with higher temperature can be transported to other points inside the droplet faster [22].

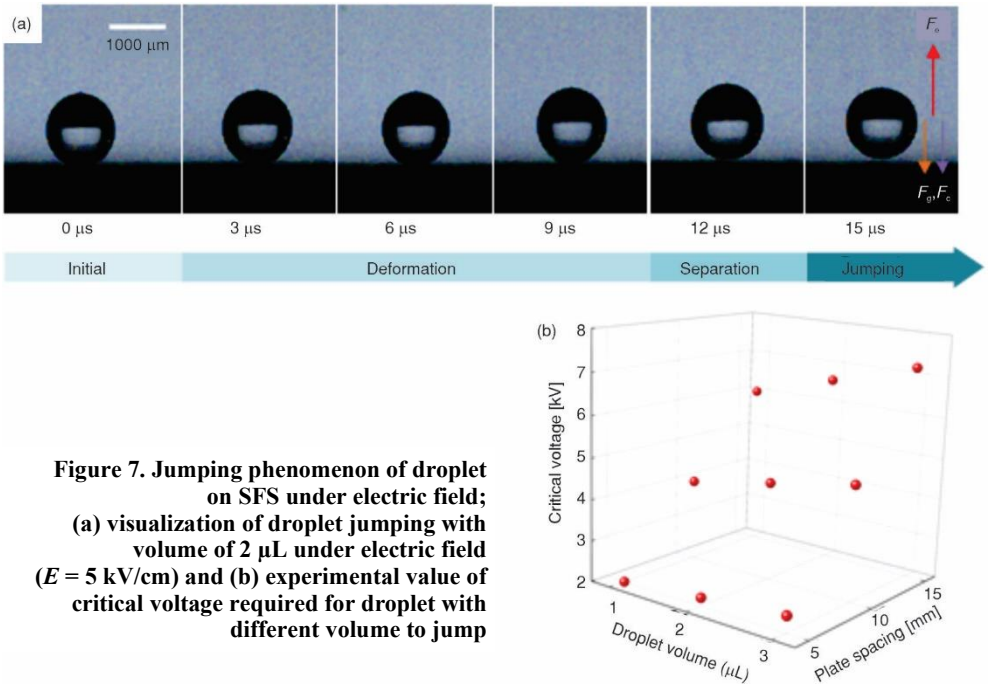

Figure 7. Jumping phenomenon of droplet on SFS under electric field; (a) visualization of droplet jumping with volume of 2 μL under electric field (E = 5 kV/cm) and (b) experimental value of critical voltage required for droplet with different volume to jump

Figure 7 shows the jumping phenomenon of droplet on SFS under electric field. In fig. 7(a), the jumping process of the droplet with volume of 2 μL under electric field (E = 5 kV/cm) is recorded. When the droplet is stretched lengthwise under the action of electric field, its contact radius also shrinks. When the contact surface between the droplet and the fin surface is

positive, the adhesion force, F_c, and the gravitational force, F_g, is not enough to maintain the force balance of the droplet, and the droplet will jump away from the fin surface under the action of electric field force, F_e. Figure 7(b) shows the experimental value of critical voltage required for droplet with different volume to jump, which is achieved by experiments. It is seen that the value of critical voltage required for the droplet to jump off SFS increases with the droplet size. Under the action of vertical electric field, the electric field force on the droplet must overcome the sum of adhesion force and gravity. Both the adhesion force and gravity increase with the increase of droplet size, and the droplet size has a greater effect on gravity than on coulomb force, so the critical voltage required for the droplet to jump away from the SFS increases with the increase of droplet size.

Conclusions

- The evaporation mode of droplet is influenced by the wettability of fin surface. The droplet evaporation on SFS is CCA and mixed modes, without the pinning stage; while it is constant contact diameter and mixed modes on BFS.
- The fin surface temperature and droplet size have no obvious effect on the evaporation mode of droplet. However, with an increase in fin surface temperature or a decrease in droplet volume, the rapid evaporation stage occurs earlier and the duration of droplet evaporation becomes shorter.
- When an electric field is applied to the droplet, the droplet shows completely different behaviors on BFS and SFS. When the electric intensity increases from 0 to 15 kV/cm, the evaporation time of the droplet with volume of 1μL is shortened by 74.6%. Moreover, the electric field forces the droplet on SFS to jump, and it is no longer necessary to remove the droplet by evaporation.

References

[1] Jiang, S., *et al*., Review and Prospect of Air Source Heat Pump Research: A Bibliometric Insight, *International Journal of Refrigeration*, *170* (2025), Feb., pp. 172-191
[2] Li, Z., *et al*., Experimental Study on the Effects of Melted Frost Icing on the Operating Performances of Air Source Heat Pump, *Applied Thermal Engineering*, *238* (2024), 122136
[3] Lyu, N., *et al*., Impact of Ambient Temperature and Humidity on the Performance of a Novel Anti-Frosting Air Source Heat Pump System, *Energy*, *314* (2025), 134190
[4] Sun, H., *et al*., Experimental Study of Active-Passive Defrosting Strategy for Heat Exchangers with Superhydrophobic Surface Modification, *Applied Thermal Engineering*, *280* (2025), 128484
[5] Li, L. T., *et al*., Investigation of Defrosting Water Retention on the Surface of Evaporator Impacting the Performance of Air Source Heat Pump during Periodic Frosting-Defrosting Cycles, *Applied Energy*, *135* (2014), Dec., pp. 98-107
[6] Malcolm, S., *et al*., Point Source Modelling Approach for Sessile Droplet Evaporation, *Physics of Fluids*, *36* (2024), 017107
[7] Shanahan, M. E. R., *et al*., Simple Theory of "Stick-Slip" Wetting Hysteresis, *Langmuir*, *11* (1995), 2, pp. 1041-1043
[8] Dietrich, E., *et al*., Stick-Jump Mode in Surface Droplet Dissolution, *Langmuir*, *31* (2015), 16, pp. 4696-4703
[9] Girard, F., *et al*., Influence of Heating Temperature and Relative Humidity in the Evaporation of Pinned Droplets, *Colloids and Surfaces A: Physicochemical and Engineering Aspects*, *323* (2008), 1, pp. 36-49
[10] Fukatani, Y., *et al*., Effect of Ambient Temperature and Relative Humidity on Interfacial Temperature During Early Stages of Drop Evaporation, *Physical Review E*, *93* (2016), 4, 043103
[11] Bin, L., *et al*., Evaporation of Methanol Droplet on the Teflon Surface under Different Air Velocities, *Applied Thermal Engineering*, *31* (2011), 17, pp. 3792-3798
[12] Carle, F., *et al*., Contribution of Convective Transport to Evaporation of Sessile Droplets: Empirical Model, *International Journal of Thermal Sciences*, *101* (2016), Mar., pp. 35-47

[13] Sefiane, K., *et al*., On the Effect of the Atmosphere on the Evaporation of Sessile Droplets of Water, *Physics of Fluids*, *21* (2009), 6, 062101
[14] Teng, L., *et al*., Evaporation of Sessile Droplet on Surfaces with Various Wettability, *Chemical Engineering Science*, *268* (2023), 118413
[15] Dash, S., Garimella, S. V., Droplet Evaporation on Heated Hydrophobic and Superhydrophobic Surfaces, *Physical Review E*, *89* (2014), 4, 042402
[16] Aldhaleai, A., *et al*., Evaporation Dynamics of Water Droplets on Superhydrophobic Nanograss Surfaces, *International Journal of Heat and Mass Transfer*, *160* (2020), 120149
[17] Xu, H., *et al*., Evaporation Characteristics and Heat Transfer Enhancement of Sessile Droplets under Non-Uniform Electric Field, *Experimental Thermal and Fluid Science*, *126* (2021), 110378
[18] Gibbons, M. J., *et al*., Evaporating Hydrophilic and Superhydrophobic Droplets in Electric Fields, *International Journal of Heat and Mass Transfer*, *164* (2021), 120539
[19] Wang, W., *et al*., Study on the Mechanism of Sessile Droplets Evaporation Enhanced by the Electric Field, *Chemical Engineering Science*, *288* (2024), 119768
[20] Kim, M. H., *et al*., A Novel Louvered Fin Design to Enhance Thermal and Drainage Performances during Periodic Frosting/Defrosting Conditions, *Energy Conversion and Management*, *110* (2016), Feb., pp. 494-500
[21] Song, M., *et al*., An Experimental Study on Even Frosting Performance of an Air Source Heat Pump Unit with a Multi-Circuit Outdoor Coil, *Applied Energy*, *164* (2016), Feb., pp. 36-44
[22] Zhang, T. H., *et al*., Numerical Simulation of Evaporation and Internal Flow of Substrate Droplet under Electric Field (in Chinese), *Chemical Industry and Engineering Progress*, *41* (2022), 2, pp. 609-618

Paper submitted: September 15, 2025
Paper revised: October 15, 2025
Paper accepted: October 16, 2025
2026 Published by the Vinča Institute of Nuclear Sciences, Belgrade, Serbia.
This is an open access article distributed under the CC BY 4.0 terms and conditions.